 doi:10.20944/preprints202203.0228.v1

Article

3D Printing and Assembling of Frame Modules Using Printable Strain-Hardening Cement-Based Composites (SHCC)

Egor Ivaniuk[1*], Martin Friedrich Eichenauer[2], Zlata Tošić [2], Steffen Müller[1], Daniel Lordick[2] and Viktor Mechtcherine[1]

[1] Technische Universität Dresden, Institute of Construction Materials, Dresden, Germany
[2] Technische Universität Dresden, Research Group Geometric Modeling and Visualization, Dresden, Germany
*Corresponding egor.ivaniuk@tu-dresden.de

Abstract: Despite all their advantages, load-bearing concrete shell structures with double curvatures are not frequently in use. The main reason is the complexity of their construction. In such a context, this article starts with a brief, critical review of existing technologies while their pros and cons are highlighted. Against that background the authors then propose a new approach for the highly automated fabrication of gridshell structures from variable modules. To demonstrate the feasibility of such a new technology, a demonstrator called ConDIT 1.0, a sphere-like shell structure composed of several frames was designed and built. The frame modules were fabricated automatically using extrusion-based 3D printing and a printable, strain-hardening cement-based composite (SHCC). This article presents the design of ConDIT 1.0, the mechanical material characterization of printed SHCC, the technology of module production, the results of geometry verification for print modules using 3D scanning, and the procedure for the demonstrator's assembly.

Keywords: concrete frames; modules; gridshell structures; 3D concrete printing; digital construction; SHCC; ECC

1. Introduction

Load-bearing concrete shell structures are highly efficient. They are created according to the principle "form follows force", so that compressive, tensile, and shear stresses act as membrane forces within the surface. Hence, such shells can be relatively thin, using a small amount of reinforced concrete. Such lightweight structures require lesser amounts of material in comparison to conventional concrete structures and make possible considerable reductions of construction-related CO_2 emission; see, e.g., [1].

Despite all the obvious advantages the use of such structures has not yet been widespread, the main reasons having to do with the difficulties in their design and construction. The fabrication of thin concrete shell structures by traditional casting requires the time-consuming creation of a unique, very expensive formwork and also leads to large amounts of industrial waste since its reuse is seldom possible [2]–[4].

An alternative approach in creating concrete shell structures is using ferrocement [5], [6]. In this technology mortar is applied over a fine metal mesh, which is attached to the main reinforcement shaped in the form of final structure. Thus, it is possible to create a structure of almost any shape, but the lack of automation makes this technology very labor-intensive.

The term flexible formwork includes a variety of different methods for creating concrete shells using flexible membranes [7]. Compared to the two previously mentioned approaches, the fabrication of shell structures using flexible formwork requires less labor, which comes, however, at the cost of less control over the structure's geometry. Mostly textile membranes are used as flexible formworks; the mortar is applied on their surfaces either by hand or using a shotcrete machine. The membranes can be pre-tensioned or freely hung, the latter frequently used in form-finding [8], [9]. New materials for

 doi:10.20944/preprints202203.0228.v1

membranes have also been developed, such as improved textiles [10], which act as reinforcement, and custom-knitted textiles [11], which allow the integration of channels and holes for reinforcement.

The membrane can also be used in combination with supporting structures to define the final geometry. For example, a membrane attached to a network of cables makes it possible to create structures of very complex shapes [4], [13], [14]. Approaches using grid shell structures as temporal support for membranes are also under development [2].

Pneumatic formwork is another type of flexible formwork technology [15]. During construction using this method, the shape of the structure is created by inflating a flexible membrane. Inflation can take place not only before the installation of the reinforcement and the application of concrete [16], but also thereafter [17], [18]. This construction method is fast, simple, and inexpensive, but the disadvantage is that the range of available geometries is severely limited. A number of studies has been carried out with the aim of diversifying the geometry of structures which can be erected using pneumatic formwork technology. It was indeed possible to achieve by the simultaneous use of several membranes [19], [20], and by their shaping [21]. The use of pneumatic formwork for erection of grid shells is also under investigation [22].

Pneumatic Forming of Hardened Concrete is a relatively new approach developed at the TU Wien [3], [23]–[25]. Similar to the pneumatic formwork method, a thin membrane is filled with air and serves as a supporting structure, but only after hardening of the concrete above it. At the same time additional post-tensioning cables are used to transform the flat plate into a double-curved shell.

Another way to create a non-linear concrete surface is to use sand or gravel hills. The Philips pavilion [26] is one example of the application of this technology. The production of concrete panels for the pavilion was very complicated and required much physical labor since the sand hills were shaped manually. The possibilities of automating this method and applying it together with 3D printing technology are currently being explored [27].

All the methods described enable the construction of concrete shells, but they are either too labor-intensive, imprecise, or are limited in their available geometries. The modularization of structures can be a solution to these problems, and a significant amount of current research is focused on this topic. The article at hand offers at first a brief overview of the research on fabrication of modular shell structures; see Section 2. Then a new approach for a fully automated fabrication of modules using strain-hardening cement-based composites (SHCC) is presented in Section 3. To demonstrate the validity of the approach and the ability to erect complex shell structures made of automatically produced modules, a demonstrator structure was designed; see Section 4. Eventually modules were fabricated and the structure was assembled as described in Section 7. The article also provides information on material design, material testing, production procedure, and quality assessment of the modules.

2. Research on fabrication of modular shell structures

The modularization of complex shapes has the potential to solve most of the existing problems of shell structures. During the design process, the structure can be divided into individual modules manufactured separately and then assembled at the construction site.

For structures with repeating geometry, the modules can be cast in conventional molds [29]. Another approach was suggested by Teng [30], in which the shell structure can be formed from steel modular units, which are afterward filled with concrete. These two technologies, however, can hardly be used for more complex geometries, in which many modules must have unique shapes.

In cases where the geometry of each module is indeed unique, one of the automated formwork production methods, such as CNC-milling or wire-cutting, can be adopted. The disadvantages of these methods are the production of large amounts of waste as well as slowness in the case of the modules with highly detailed surfaces. The waste problem

Preprints (www.preprints.org) | NOT PEER-REVIEWED | Posted: 16 March 2022 doi:10.20944/preprints202203.0228.v1

could be resolved by using wax to create formwork, which is completely reusable [31]. The use of vacuumatic formwork [32] is another approach for production of waste-free, reusable molds.

CASTonCAST is the method for the production of shell structure modules developed at ETH Zurich [33]. In this method, the modules are produced stacked on top of each other, so one module defines the shape of the other module located above it, thereby eliminating the need for complex formwork. Construction using stackable modules requires a special method for the design of the freeform shapes.

Adjustable formwork is one of the most technologically advanced methods of creating curved modules for shell structures [35]–[41]. Most commonly such a formwork consists of vertical beams which can be moved in the vertical direction to bent a flexible surface lying on top of the beams. The movement of the beams is usually driven by motors, but this can also be done using a robotic arm [42]. In most of the designs of adjustable formwork developed, the shape of the module is controlled by the flexible surface only from one side, but there also exist prototypes with double-sided control [43], where the flowable concrete can be filled inside, as in a conventional mold.

In the case of one-sided adjustable formwork, the flowable concrete is poured onto a flat surface that deforms after the concrete is slightly hardened to prevent it from flowing. Flexible bands can be used to define the edges of the manufactured module, the position of which can be determined using a laser projection [44], [45]. After deformation of the flexible surface, the module reaches the required geometry and is left to lie on the formwork until it is completely solidified. The impossibility of further use of the adjustable formwork before the concrete hardens greatly reduces the productivity of this technology. In an attempt to change this, TU Eindhoven developed the technology "VaCo Mould" [46], in which they used adjustable formwork and vacuum forming to produce double-curved plastic molds for concrete casting.

The use of adaptive formwork is a promising approach to producing modules for the construction of sophisticated, double-curved shells. However, adaptive formwork is complex and, hence, difficult to manufacture and use. In fact, the method has been used previously, albeit mainly in research projects. Recently, manufacturers of these devices have entered the market, thereby making the technology more accessible to the construction industry; see, e.g., [47].

Recently, studies have also been conducted on the use of 3D concrete printing technology for the creation of shell structure modules. In the research of Lim *et al*. [49] a double-curved shell element was produced using this technology. The possibility of combining adjustable formwork and 3D concrete printing was also investigated [50]. In these two mentioned research works, printing was performed by the extrusion of fine concrete filaments, which offered adequate accuracy but resulted in a relatively long printing time.

In the study by Borg Constanzi *et al*. [51], only the outer edges of the elements were 3D printed, which significantly reduced printing time. After printing, the inner portions of the elements were filled with fresh concrete. Both 3D printing and concrete casting were performed on CNC-milled formwork; the use of this approach in combination with adjustable formwork was also proposed.

3. Proposed technology

In this article the authors propose an alternative approach in the production of shell-structural modules without formwork. The new approach combines the technology of full-width 3D concrete printing using highly ductile SHCC material [52], [53] and the technology of robotic textile mesh production, particularly that using mineral-impregnated carbon yarns [54]. SHCC seems to be very suitable for producing the edge zones of the modules. This choice of material ensures not only that high load-bearing effects and dimensional stability are achieved, but also that very large local stresses, e.g., during transport and assembly, such as tilting, impact, or in connecting the modules, can

Preprints (www.preprints.org) | NOT PEER-REVIEWED | Posted: 16 March 2022 doi:10.20944/preprints202203.0228.v1

be sustained. In addition, the entire construction would then show "good-natured" load-bearing deformation behavior in the event of an unplanned local or global overload through redistribution of forces or stresses. For the infill, concrete reinforced with continuous fibers / textile appears to be the best choice, since such reinforcements enable thin-walled, lightweight, material-saving, but also fully automated solutions. **Error! Reference source not found.** shows the production steps of a module with a filled inner zone.

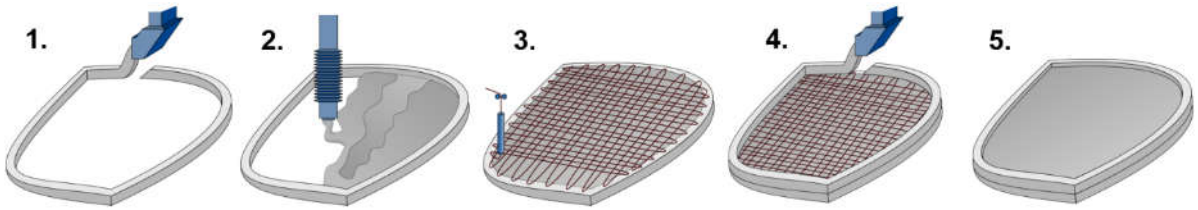

Figure 1. Production steps.

The production is divided into five sub-processes, depending on the working tool used. In the first step, SHCC is extruded at the edge zone of the module using a 3D printer. The positioning of a printer is computer-controlled and fully automated. In the second step, the inner part of the module is filled with concrete, which can be pumped, sprayed, or poured, depending on the concrete type in use and the available machinery. The third step is reinforcing with a carbon textile mesh. This material was chosen due to its high tensile strength and durability [55], [56]. Additionally, the fiber material is characterized by high chemical resistance. Because of this, the concrete cover can be reduced to a few millimeters, which enables the production of very thin structures. In the fourth step, the second layer of the outer edge is printed. To complete the module production, in the fifth step the area within the printed edges is filled with concrete.

Within a module, the textile mesh serves not only as reinforcement, but also provides an additional bond between the outer edge and the infill. It can also be used in connecting the modules. This could be done either with embedded metal elements or with a direct mesh-to-mesh connection. For a second approach the textile meshes should be placed to extend beyond the boundaries of the modules. During assembly, the meshes of neighboring modules could be joined together, providing continuous reinforcement throughout the entire structure.

Textile mesh could be prefabricated, or it could be directly custom produced on the respective module using robots, as shown in the example in **Error! Reference source not found.**. Fully automated placement of the textile yarns using a robotic arm was demonstrated at the TU Dresden previously [54]. Shortly before and directly during the mesh production, yarns should be coated with a mineral micro-suspension, which considerably enhances its bond to the concrete matrix und the performance of the reinforcement at elevated temperatures [57].

Since each of the steps described can be done by robots, the whole process can be automated. For mass production a conveyor system can be implemented: a platform with a module moves from one station to another, where all the production steps are carried out in sequence. The technology does not require any pauses between the steps. At the end of production, the platform with the completed module can be transported to a storage room for the curing of the concrete.

The separation of the modules into inner and outer zones provides great design freedom. The modules could as well be produced without concrete infill. The inner zones of the modules can be used for the integration of solar panels or other technical equipment. The integration of windows into modules increases the natural illumination of the area within the structure, thereby eliminating the opacity problem inherent in concrete shells [58]. For the modules without infill, textile reinforcement can be placed only along the outer edge. **Error! Reference source not found.** presents a design of a space frame bridge

Preprints (www.preprints.org) | NOT PEER-REVIEWED | Posted: 16 March 2022 doi:10.20944/preprints202203.0228.v1

– one of the possible applications for modules without infill. The present article is concentrated on production of such modules without infill.

The assembly of the modules into the final shell structure can be performed using traditional methods such as scaffolding and cranes. Pneumatic forming technology [59], [60] also can be adopted in cases where the geometry of the shell structure can be completely or partially represented with inflatable membranes.

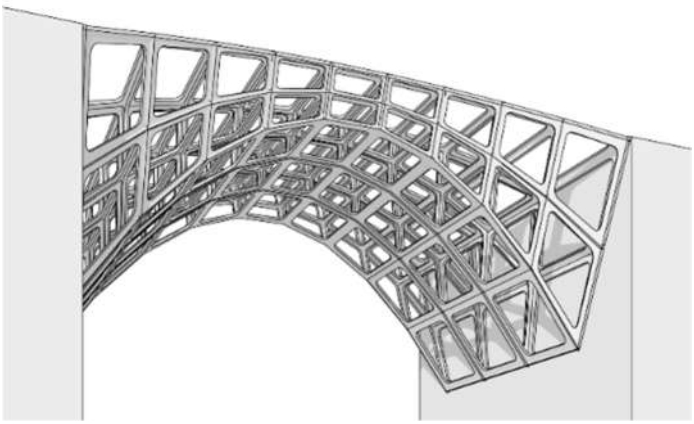

Figure 2. Design of a space frame bridge [D. Lordick 2020].

4. Design of a demonstrator

The demonstrator was designed according to the idea of reducing the complexity of general grid shells while certain aspects of the fabrication approach were tested under laboratory conditions. However, the strategies used for developing the demonstrator are still scalable to the assembly of general gridshells and to the automation of the processes.

4.1. Design constraints

The concept of wide-span and lightweight gridshell structures as explored here typically involves planar quadrilateral (PQ) modules. So-called PQ-meshes can approximate a great variety of freeform surfaces. Therefore, it is not a major limitation with respect to the overall structure that the 3D concrete printing, i.e., production steps 1 and 4, at this stage uses only a flatbed for material deposition; see **Error! Reference source not found.**.

Gridshells from glass and steel typically require diagonal cables, which stiffen the quadrilaterals. The approach here is to generate inherently stiff modules and avoid additional diagonal elements. Thus, the individual frames are formed with a profile that can sustain bending moments. The cross-section of the profile is chosen depending on the capacity of the extruder nozzle. The size of the module should be chosen to be large enough to allow reasonably long edges between the rounded corners and still fit on the flatbed of the 3D printer.

Freeform structures usually require individually formed quadrilaterals. The challenge of dealing with geometrically variable individual frames is being addressed in ongoing work. Here, as a first step, a series of identical frames must be generated and examined to measure precision and repeatability. So long as the frames are reasonably reproducible, it is predictable that individual parts can be created with similar precision.

4.2. The Polyhedron

For the reasons described above, the demonstrator is composed of congruent quadrilaterals. This boundary condition quite naturally suggests the introduction of a sphere-like polyhedron. Such polyhedrons have the additional advantage that they do not require a support structure, but function as independent objects. Last, but not least, the assembly of the elements into a closed polyhedron shows whether the accuracy is sufficient.

Preprints (www.preprints.org) | NOT PEER-REVIEWED | Posted: 16 March 2022 doi:10.20944/preprints202203.0228.v1

There is a short list of possible candidates, starting with the cube and its six faces, considered trivial. Others are the rhombic dodecahedron with 12 faces and the rhombic triacontahedron with 30 faces. Both have the disadvantage of highly symmetric quadrilaterals, which are, however, too special with respect to further applications in gridshells. Only the deltoidal icositetrahedron with its 24 kite-like faces meets the requirements; see **Error! Reference source not found.**a. An acronym of the Greek name in connection with an abbreviation of concrete provided together the name ConDIT for the demonstrator. The version number 1.0 is meant to indicate that future steps of testing could involve refined versions of the basic design. In fact, ConDIT 1.0 has a precursor in BenDIT, a structure made of bent wood [61].

4.3. The connectors of the modules

The dihedral angles of the deltoidal icositetrahedron are all the same. This offers the chance to equip all edges of the modules with identically beveled sides and join them seamlessly. Such a solution will be addressed in the following research. The modules of ConDIT 1.0 are instead equipped with straight edges, which makes a gap between the faces/modules necessary. The gaps are bridged with connectors, which are stuck into the first layer of fresh concrete before the second layer is added. As such, the 96 connectors, two at each at the 48 edges, are each made of two parts, which are joined with a screw during assembly. This enables the pre-assembly of module groups on a flat surface before their being bent into a spatial configuration.

The connecting parts are simple metal fittings for wooden structures obtainable at a hardware store and adjustable by cutting away a small piece and extended by screws which are fixed in the concrete; see **Error! Reference source not found.**b. Since the modules of ConDIT 1.0 are joined with 96 screws, the whole structure can easily be dismantled. For presentation it is esthetically preferable if the structure is suspended from a ceiling; see **Error! Reference source not found.**c. The suspension should lift ConDIT 1.0 at a vertex where only three modules meet. Seen thus, the object presents a three-fold symmetry, which corresponds to that of an inscribed cube with a vertical diagonal.

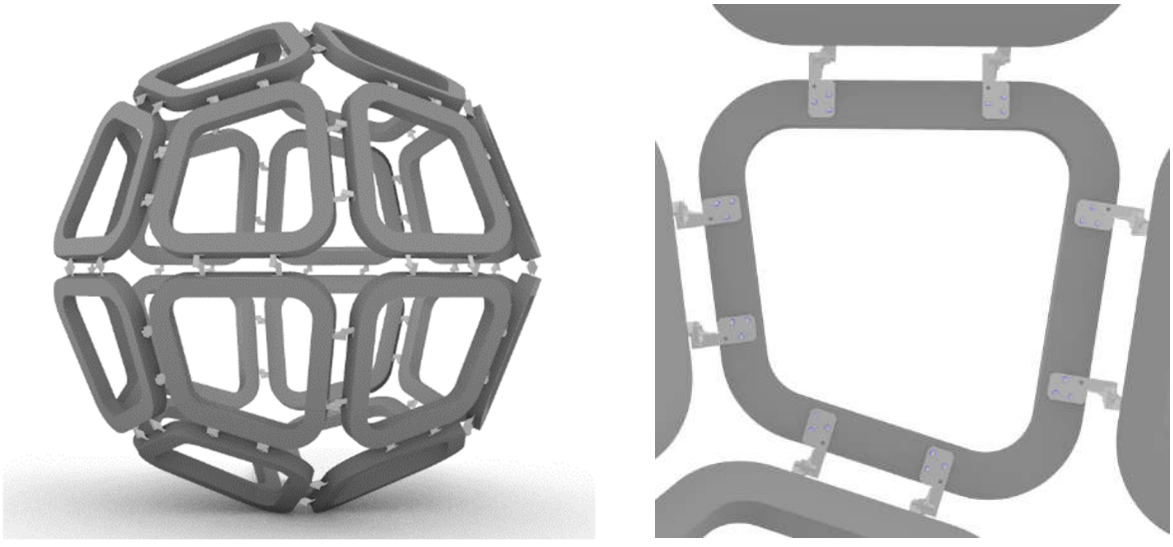

a) **b)**

Figure 3. a) Design of the demonstrator, and **b**) design of the connectors between the modules.

5. Experimental program

5.1. Materials and mixing procedure

To be able to withstand the loads acting between individual modules, the material of the outer edge should possess not only high resistance to compression but also to tension.

Preprints (www.preprints.org) | NOT PEER-REVIEWED | Posted: 16 March 2022 doi:10.20944/preprints202203.0228.v1

For this reason, strain-hardening cement-based composite (SHCC), reinforced with short polymer fibers, was chosen as construction material. This material is characterized by its high material strength, ability to withstand significant deformation, and high energy absorption capacity. Additionally, short fibers prevent the occurrence of cracks due to plastic and drying shrinkage. This property is essential for the 3D printed material which is not covered by the formwork as in conventional construction, and hence, subject to increased drying effects. The choice of this material ensures that high local stresses which could arise during transportation, assembly, and construction can be absorbed.

There are several scientific publications in which SHCC was developed especially for 3D printing [52]. The mixture developed by Ogura *et al*. [53] is taken here as the basis of the composition used. Due to its relatively low fiber content and short fiber length, this mixture has the best printing quality in comparison to other mixtures presented in the literature. To achieve better control over cement constituents, the cement CEM II/A-M (S-LL) 52.5 R, which was used in the original mixture, was replaced with CEM I 52.5 R (80 %) and Saxodol 90 LE (20 %). Saxodol 90 LE is a white marble powder with a maximum grain size of 90 μm. It was used as a partial replacement of cement to obtain a similar amount of clinker as in the original mixture composition. Also, the dosage of superplasticizer was reduced to achieve a similar cone spread diameter. **Error! Reference source not found.** shows the SHCC mixture composition under investigation.

Table 1. SHCC mixture composition under investigation.

Component	Type	Producer	Mass [kg/m^3]
Cement	CEM I 52.5R ft	Holcim	913.9
Marble powder	Saxodol 90 LE	sh minerals GmbH	228.5
Fly ash	Steament H-4	STEAG P.M.	152.3
Microsilica (50% suspension)	EMSAC 500E	BASF	457.0
Sand 0.06-0.2	BCS 413	-	91.3
Sand 0-1	Ottendorf sieved	-	213.1
Water	Tap water	-	106.6
Superplasticizer	MasterGlenium SKY593	BASF	16.8
Fibers	PE 6 *mm*	Eurofibers	15.3

All SHCC batches were prepared using a Zyklos Rotating Pan Mixer and following the same procedure. First, dry materials, i.e., cement, marble powder, fly ash, and sand, excepting the fibers, were mixed for 2 minutes, keeping a rotating speed constant at 30 rpm. After that, without interrupting the mixing, liquid components were added, i.e., microsilica suspension and water mixed with a superplasticizer. The addition process took approximately one minute. One additional minute of mixing was required to obtain a flowable paste, afterwards, the mixer rotating speed was increased to 50 rpm. As the next step, again without stopping the mixer, PE fibers were gradually added, which took around two minutes. Eventually, the mixture with all the components was mixed for two additional minutes to achieve uniform fiber distribution.

5.2. 3D printing tests, production of specimens

A frame concrete printer developed at the TU Dresden was used for the 3D printing experiments; see **Error! Reference source not found.**. With a printing area of 1.4 *m* x 1.0 *m* and with a maximum printing height of 1.2 *m*, the printer is capable of production of modules for large shell structures.

Preprints (www.preprints.org) | NOT PEER-REVIEWED | Posted: 16 March 2022 doi:10.20944/preprints202203.0228.v1

Figure 4. 3D concrete printer used in this investigation.

At the beginning of this investigation, a series of printing tests were conducted with the aim of finding a nozzle geometry capable of filament extrusion with a rectangular cross-section, which is necessary for the fabrication of the ConDIT 1.0 modules. Later the nozzle chosen was used in the final printing test, which was performed to evaluate the printability of the modified SHCC mixture composition.

Given that the material supply to the printhead works well, the printability can be characterized by two parameters: extrudability and buildability. Extrudability is the ability of a material to be sustained in continuous flow during the extrusion; a 3D printing test is the most straightforward approach to evaluate this parameter. The second parameter, buildability, is the property of an extruded material to retain its geometric shape under the influence of increasing load. The load consists of the weight of the layer itself and the weight of subsequent layers. In the case of a nozzle with vertical orientation, the extrusion pressure additionally acts on the already deposited layers. In the proposed technology, the outer edge of the module consists only of two layers of material. Hence, the printing of two-layer walls during the 3D printing test was sufficient for verification of buildability.

During the final 3D printing test, straight walls of 1 and 2 layers were printed for the purpose of material testing; see **Error! Reference source not found.**b. One-layer walls were used for production of the specimens used in the uniaxial tensile test. From the two-layer walls the prism specimens for bending tests and cube specimens for compression tests were cut out; see **Error! Reference source not found.**.

According to previous research the fibers orient themselves as they pass through the 3D printer [52], [53], which affects the mechanical properties of the material. Therefore, this method of specimen preparation allows more accurate determination of the strength parameters of the SHCC subjected to extrusion when compared to the specimens produced using the conventional method of mold-casting.

Preprints (www.preprints.org) | NOT PEER-REVIEWED | Posted: 16 March 2022 doi:10.20944/preprints202203.0228.v1

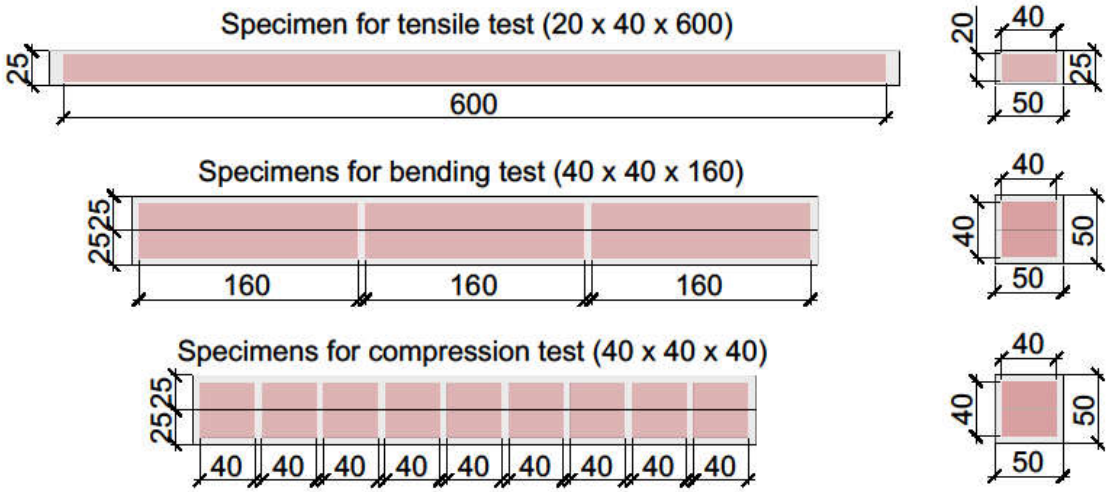

Figure 5. Scheme of cutting specimens from printed walls.

5.3. Bending and compressive tests

Machine-controlled, three-point bending tests were performed on specimens at concrete ages of 1 and 7 days. Specimens for the 7-day tests were stored in a climate chamber wrapped in a plastic film. Prisms with dimensions of 160 *mm* x 40 *mm* x 40 *mm* were cut out from the printed walls on the day after printing. For all the tests, the same experimental setup was used, with the distance between the bottom supports equal to 120 *mm*. Specimens were loaded monotonically with a constant displacement rate of 1 *mm/min*. Bending tests were performed in two directions, D1 and D2, both perpendicular to the printing path, as shown in **Error! Reference source not found.**. The blue line indicates the top surface of the printed wall and is oriented along the printing path.

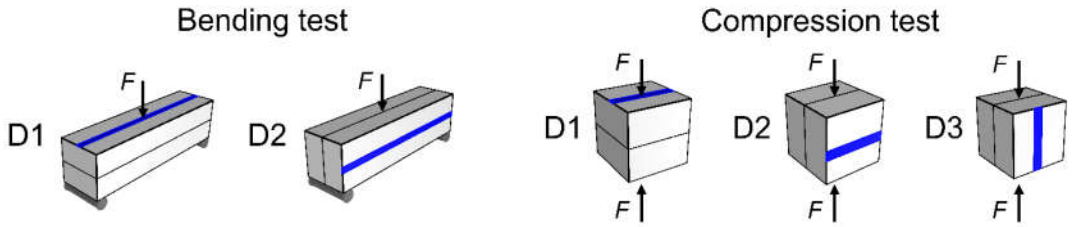

Figure 6. Loading directions in bending and compression tests.

Compression tests were performed on the cubes with an edge length of 40 *mm*. As was done for the bending tests, specimens were cut out from the printed walls the day after printing, and specimens for testing at 7 days were stored in a climate chamber wrapped in a plastic film. Material behavior under compression was investigated in three different directions: D1 and D2 are perpendicular to the printing path, and D3 is parallel thereto, as presented in **Error! Reference source not found.**.

5.4. Uniaxial tensile tests

Uniaxial tensile tests were conducted on specimens at the age of 7 days. For each specimen, a rectangular prism with dimensions of 600 *mm* x 40 *mm* x 20 *mm* was cut out from the printed wall and placed into a formwork, as shown in **Error! Reference source not found.**a. Following that the empty space at both ends of the formwork was filled with fresh SHCC. On the next day the specimen was demolded, and the surfaces were polished. This procedure enabled the obtaining of specimens with the desired dumbbell shape, required to prevent premature specimen failure in the vicinity of the machine grips.

Tensile tests were performed in a deformation-controlled regime with a constant displacement rate of 1 *mm/min*. The deformation was measured over a length of 150 *mm* in

Preprints (www.preprints.org) | NOT PEER-REVIEWED | Posted: 16 March 2022 doi:10.20944/preprints202203.0228.v1

the middle portion of the specimens by two Linear Variable Differential Transformers (LVDTs). The experimental setup is presented in **Error! Reference source not found.**b.

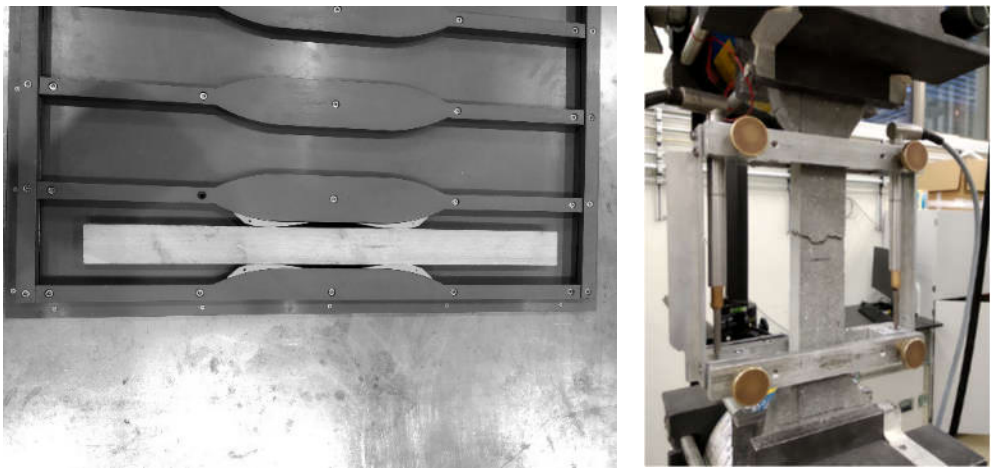

a) **b)**

Figure 7. a) Production of dumbbell specimens for tensile tests, and **b**) tensile test setup.

5.5. Connector pullout test

To verify the strength of the bond between the connectors and the SHCC, a series of pullout tests was performed. The specimens for testing were cut directly from the printed modules. On each specimen the area around the connector was polished after cutting; see **Error! Reference source not found.**a. This was done to ensure a tight fit with the metal ring holding the specimens during the test. The test setup is presented in **Error! Reference source not found.**b. Pullout tests were performed at a constant displacement rate of 2 *mm/min*.

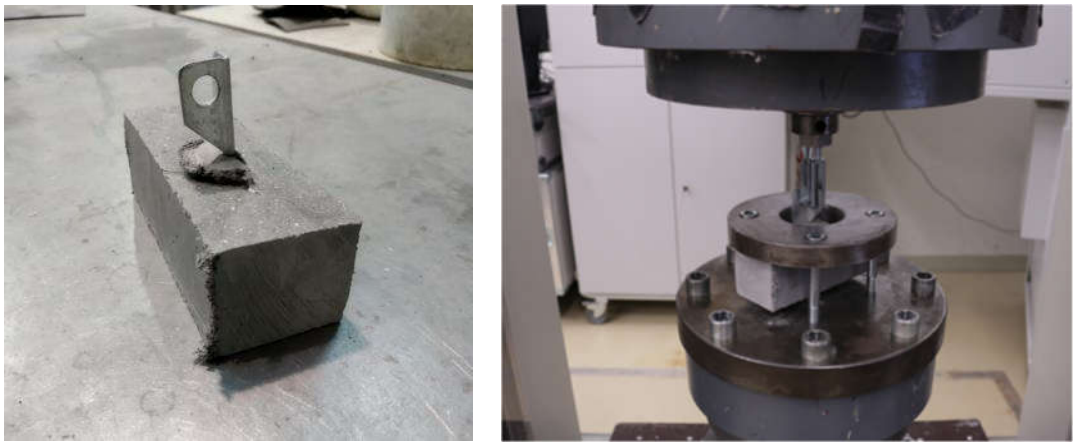

a) **b)**

Figure 8. a) Specimen for a connector pullout test, and **b**) pullout test setup.

5.6.3D scanning of printed modules

The fabrication of the modules for ConDIT 1.0 was carried out using the printer described in Section 0. A few weeks after, when the largest shrinkage deformations had already been completed, each module was scanned using a structured-light 3D scanner Artec Eva; see **Error! Reference source not found.**a. This is a handheld device with an accuracy of up to 0.1 mm and a resolution of up to 0.2 mm.

Preprints (www.preprints.org) | NOT PEER-REVIEWED | Posted: 16 March 2022 doi:10.20944/preprints202203.0228.v1

During the scanning a cube with a side length of 95 mm was placed in the center of the scanned module as shown in **Error! Reference source not found.**b. It was used as a scaling reference during the analysis of the scan results. Each module was scanned twice: once from the top and once from the bottom. Geometries of the modules obtained with the scanner were compared with the geometry defined by the design. Parameters such as inconsistency of geometry, surface roughness, and accuracy of connector positioning were analyzed.

a) **b**)

Figure 9. a) Structured-light 3D scanner Artec Eva [source: www.artec3d.com], and **b**) the setup for module scanning.

6. Experimental results

6.1. 3D printing tests

As mentioned above, for production of ConDIT 1.0 modules the extruded filament should have a rectangular cross-section. A nozzle with a vertical orientation was preferred because it allows printing the layers with an enclosed shape, where the start and end-points are the same. In contrast to this, horizontally oriented nozzles must be lifted at the end of the enclosure so as not to damage the already printed structure, and extrusion must be performed a certain distance from the printing surface.

The vertically oriented circular nozzle commonly used in concrete 3D printing was used in the initial experiment and yielded poor surface quality of the extruded filaments and demonstrated its inability to form the required cross-sectional shape. The addition of side trowels to this nozzle allowed achievement of a flat surface on the sides of the printed walls. However, the necessary shape of the cross-section still was not achieved since the top surface of the printed layer had a wavy structure; see **Error! Reference source not found.**a.

In the next test printing the outlet cross-section was changed to a rectangular one with dimensions 55 *mm* x 25 *mm*. In addition to the side trowels, the new nozzle was also equipped with a top trowel; see **Error! Reference source not found.**b. To decrease the adhesion between the trowels and printed material, the inner sides of the trowels were shielded by metal plates. With this nozzle it was possible to achieve smooth top and side surfaces; see **Error! Reference source not found.**a. Eventually, it was used in the final 3D printing test and for production of the ConDIT 1.0 modules.

Preprints (www.preprints.org) | NOT PEER-REVIEWED | Posted: 16 March 2022 doi:10.20944/preprints202203.0228.v1

a) **b**)

Figure 10. a) The layer extruded using a vertically oriented circular nozzle with side trowels, and **b**) vertically oriented rectangular nozzle with side and top trowels.

During the final 3D printing test the chosen SHCC mixture showed good extrudability. All the printed layers were extruded continuously, without gaps, as can be seen in **Error! Reference source not found.**b. A slight deformation of the bottom layer was noticed during the printing of the second layer, which occurred mainly due to the pressure of extrusion. Otherwise, the printed walls were able to maintain their shape, no additional deformation was observed. The results of the test confirmed the adequacy of this material and the nozzle as developed for printing ConDIT 1.0 modules.

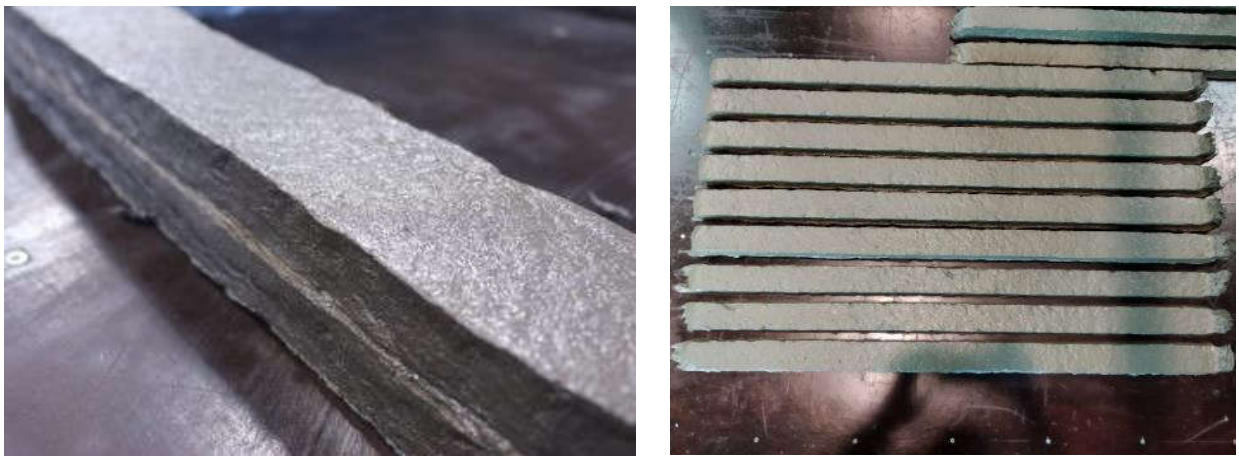

a) **b**)

Figure 11. a) The wall extruded with vertically oriented rectangular nozzle with side and top trowels, and **b**) walls printed during final 3D printing.

6.2. Bending and compressive tests

The force-displacement diagrams obtained during the bending tests for the 1-day and 7-day specimens are presented in **Error! Reference source not found.**a and **Error! Reference source not found.**b, respectively. As can be seen from the graphs, the specimens showed similar behavior in both loading directions. The values of ultimate flexural strength are only slightly superior for the direction D2; see Table 3. This similarity in the results can be explained by the good bond between the printed layers and by the even distribution of the fibers over the cross-section of the extruded layers. Indeed, after

Preprints (www.preprints.org) | NOT PEER-REVIEWED | Posted: 16 March 2022 doi:10.20944/preprints202203.0228.v1

specimen cutting, it was not possible to visually determine the position of the interface zone between two printed layers. The short time interval between the printing of the layers, the sufficient flowability of SHCC under investigation, and the additional pressure during extrusion due to the vertical orientation of the nozzle are the reasons for the good adhesion between the layers.

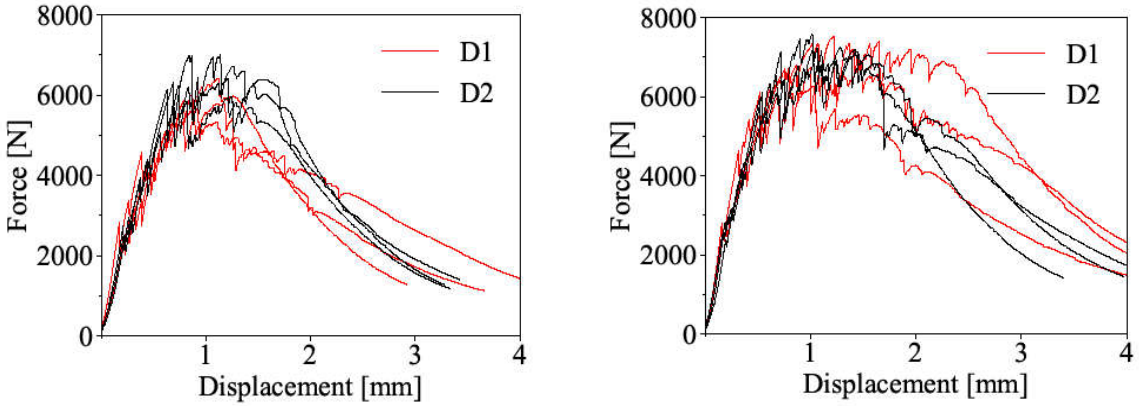

Figure 12. Bending tests results for the specimens of concrete age **a**) 1 day, and **b**) 7 days.

Good fiber distribution was also confirmed by examination of the specimens with a microscope; see **Error! Reference source not found.**a. A certain degree of fiber orientation parallel to the printing direction was observed on the side view of the specimen's cross-section; see **Error! Reference source not found.**b.

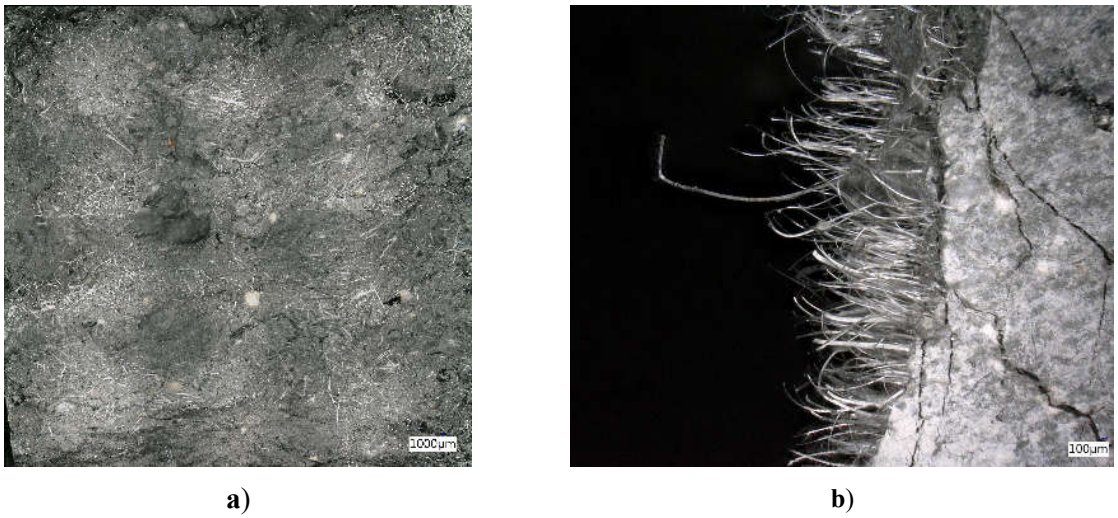

Figure 13. Microscope photos of a SHCC specimen after failure in the bending test: **a**) the top view on a fracture surface, and **b**) the side view.

Table 2. Ultimate flexural and compression strength.

Direction	Flexural strength [MPa]		Compression strength [MPa]	
	1 day	7 days	1 day	7 days
D1	14.0 (0.8)	15.8 (1.1)	32.9 (0.7)	54.8 (2.2)
D2	15.3 (1.1)	17.1 (0.6)	32.5 (0.1)	56.1 (7.6)
D3	-	-	36.2 (0.9)	61.2 (4.8)

Preprints (www.preprints.org) | NOT PEER-REVIEWED | Posted: 16 March 2022 doi:10.20944/preprints202203.0228.v1

The results obtained from the compression tests are presented in **Error! Reference source not found.**. The values of compressive strength for the specimens tested in direction D1 and D2 are practically equal, while the values of the test results in direction D3 slightly exceed them. Fiber orientation could be the reason for this discrepancy. Directions D1 and D2 both are perpendicular to the printing path, the main direction of fiber orientation, while direction D3 is parallel to it.

6.3. Uniaxial tensile tests

Stress-strain diagrams obtained from the uniaxial tensile tests are presented in **Error! Reference source not found.**a. As can be seen, the specimens showed pronounced strain-hardening behavior. Under uniaxial tensile loading, multiple fine cracks formed on the specimens' surfaces. The first cracks appeared at a tensile stress of around 3 *MPa*. The composite yielded a strain capacity of approximately 2% when reaching the maximum tensile stress of 4.7 *MPa* at the average.

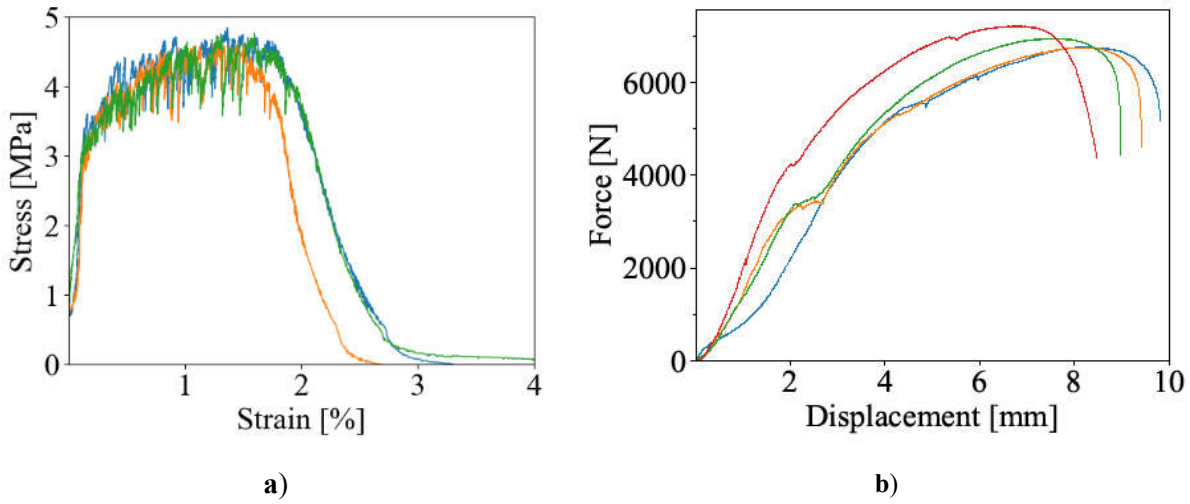

Figure 14. a) Tensile test stress-strain diagram, and **b**) the results of connector pullout tests.

6.4. Connector pullout test

The results of the connector pullout tests are presented in **Error! Reference source not found.**b. During the experiments, specimens demonstrated good bonding between the connectors and the SHCC. In all the tests, breakdown of the specimens appeared due to the failure of the metal; see **Error! Reference source not found.**a, while no significant deformation or cracks were observed at the connector/SHCC-interface zones around the pins; see **Error! Reference source not found.**b.

Preprints (www.preprints.org) | NOT PEER-REVIEWED | Posted: 16 March 2022 doi:10.20944/preprints202203.0228.v1

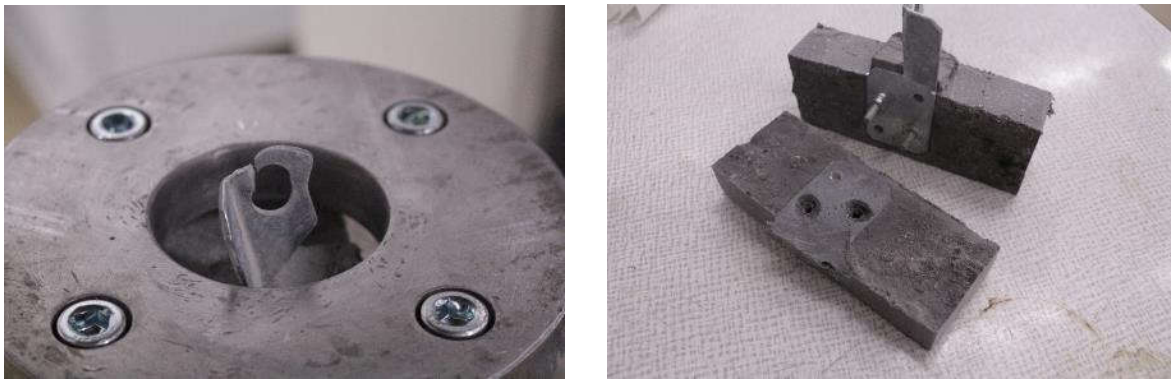

a) **b**)

Figure 15. a) Typical failure of a metal connector during pullout test, and **b**) specimen after pullout tests, split into two parts.

7. Production of the demonstrator

7.1. 3D printing process

Production of the ConDIT 1.0 modules consisted of three steps. In beginning, the first layer of the outer edge was printed. As the second step connectors were installed manually by pressing them into the fresh material of the just-printed layer. The final step was the printing of the second layer of the outer edge.

To place the connectors in the right positions, the frame with the shape of the module was used, which had marked connector locations on it. It is worth noting that the connectors should be well pressed into the bottom layer. Otherwise, they may be displaced during the printing of the second layer.

It took about 5 minutes to make one module. The printing of modules was performed on separated platforms, so that after production it was possible to bring a platform with the already manufactured module to the storage room and free the printing zone for production of the next.

7.2. 3D scanning of the modules

As stated earlier, two scans were made for each of the modules produced – one from the top and another from the bottom side of the module. In total, 48 scans were made. The data obtained during 3D scanning was in the form of STL files. Three programs were used for the processing of the files obtained. The first step was done in *MATLAB*, during which the module and the scaling cube were isolated by removing the points that represented the surface on which the scanned elements were placed; see **Error! Reference source not found.**.

Preprints (www.preprints.org) | NOT PEER-REVIEWED | Posted: 16 March 2022 doi:10.20944/preprints202203.0228.v1

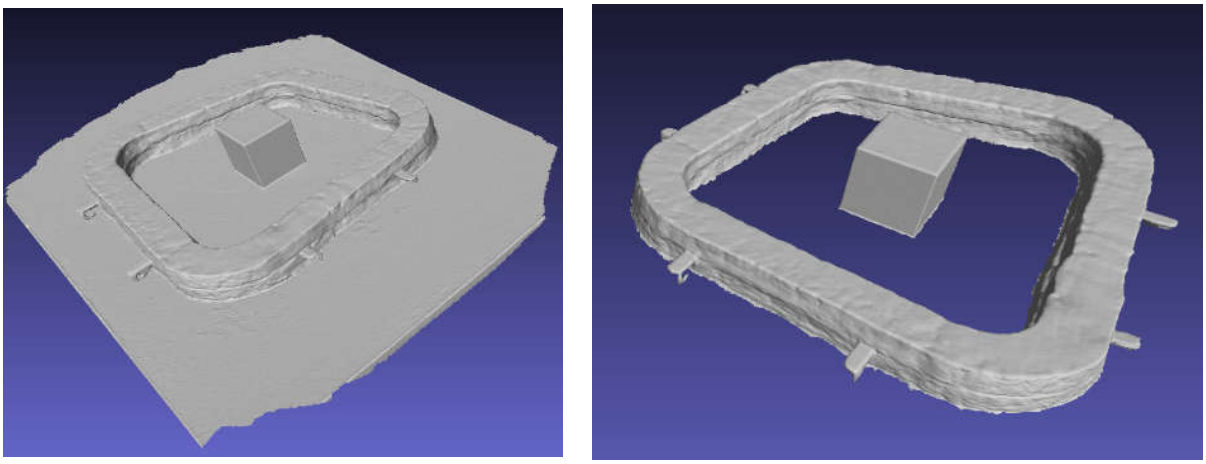

a) **b**)

Figure 16. The results of 3D scanning **a**) initial results, and **b**) after deleting the excess surfaces in MATLAB.

In the second step, the geometry of the cube obtained and the module were imported in *Rhino* for scaling. This step was necessary because a difference was found between the scanned results and the true dimensions of the cube. During the processing, the module and the cube were scaled in such a way, that the scanned cube matches its real dimensions. To measure the scanned edges of cubes as precisely as possible, the intersections of the side planes of the cube were found with *Grasshopper*, a *Rhino* plug-in.

As the last step, the file with the geometry of the scaled module was transferred to the program *CloudCompare*, where it was compared with the designed geometry. In this program, the data was transformed from meshes to point clouds, and geometries of the scanned and the designed modules were overlapped using the option for "aligned entities".

The accuracy of the printed modules' geometries was the first parameter for evaluation. An example of the result for one of the modules is shown in **Error! Reference source not found.**. The figure represents the geometry of the printed module, the color on the surface of which denotes the geometry accuracy. The geometry accuracy of each point on the surface was calculated as a distance between this point and a matching point of the designed module geometry. The colors and corresponding distances, indicated in *mm*, are shown on the scale located on the right side of the figure. The maximum deviations for this module can be observed in the certain areas, and can reach values of about 10 *mm*. The first is at the bottom of the element, where the module was adjacent to the platform. The second area is in the border zone between two printed layers. Similar results were obtained for other modules as well. This can be explained by the presence of a small gap between the nozzle trowels and the printed surface during the printing, through which the printed material could flow under the pressure of extrusion. To avoid this effect, in future it is planned to print modules with a decrease in the printing speed, thereby reducing the extrusion pressure, and to develop a less flowable, but still extrudable material. The use of post-processing techniques such as milling is also one of the possible ways to increase the accuracy of the module geometry.

Preprints (www.preprints.org) | NOT PEER-REVIEWED | Posted: 16 March 2022 doi:10.20944/preprints202203.0228.v1

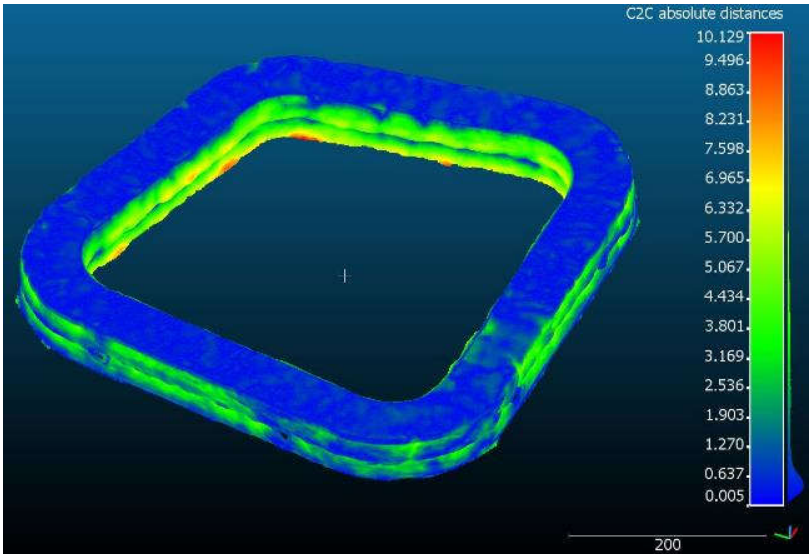

Figure 17. An example of the result of geometry accuracy evaluation for one module.

The results of measurements of geometry accuracy for all the modules were combined separately for the scans from the top as seen in **Error! Reference source not found.**a, and from the bottom of the modules, as seen in **Error! Reference source not found.**b. Diagrams show a higher geometrical accuracy for the scans from the bottom of the modules, which was expected, since the bottom surface of the module is shaped during the extrusion by the flat printed bed and is protected from moisture evaporation during SHCC-hardening.

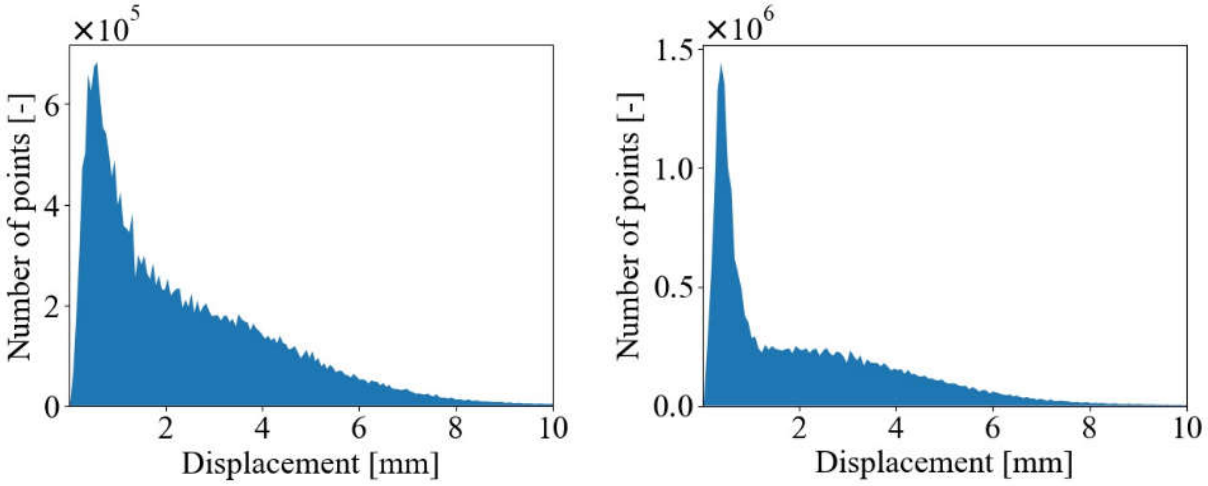

a) **b**)

Figure 18. Combined diagrams of geometry accuracies for all the modules scanned from **a**) the top, and **b**) from the bottom.

Surface roughness was the second characteristic measured. This parameter became important since it was noticed that the surface smoothness greatly decreases on the day after production due to the setting/plastic shrinkage of the SHCC under investigation. More information on plastic shrinkage of printed cement-based materials can be found in [62]. Thus, by measuring surface roughness it was possible as well to assess the shrinkage effects to some extent. The measurements were performed separately for the top and bottom parts of the modules. The value of roughness was calculated as the distance between the tested point and the plane of the surrounding vertices. **Error! Reference source not**

Preprints (www.preprints.org) | NOT PEER-REVIEWED | Posted: 16 March 2022 doi:10.20944/preprints202203.0228.v1

found. presents the result of the top surface roughness evaluation for one of the modules. The scale on the right side of the figure shows the colors with the corresponding values of surface roughness in *mm*.

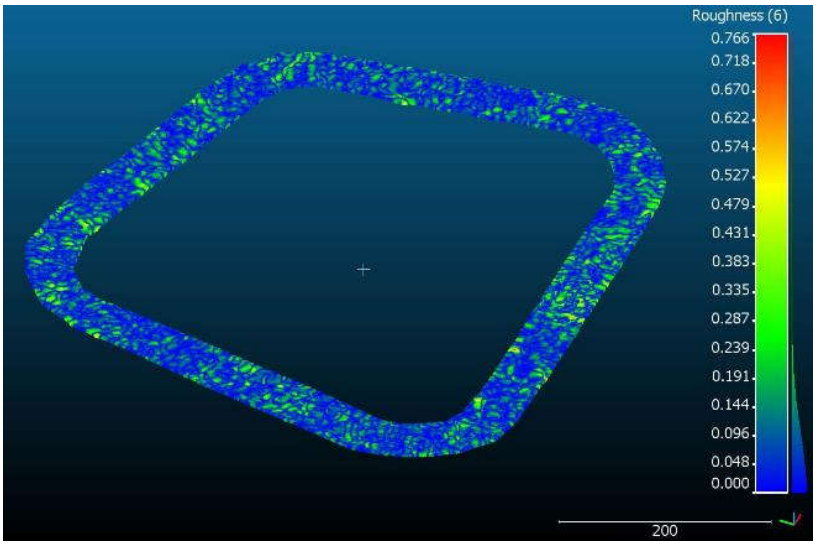

Figure 19. A representative result of surface roughness assessment for a module.

The summarized results of all the modules for the top and the bottom surfaces are shown in **Error! Reference source not found.**a and **Error! Reference source not found.**b, respectively. For most of the points, the values of surface roughness of the top surface are lower than 0.4 *mm*, while the values for the bottom surface for most of the points do not exceed 0.1 *mm*. In the future, it is planned to reduce the surface roughness by improving the nozzle, and by enhancing the printed material formulation, making it less prone to shrinkage.

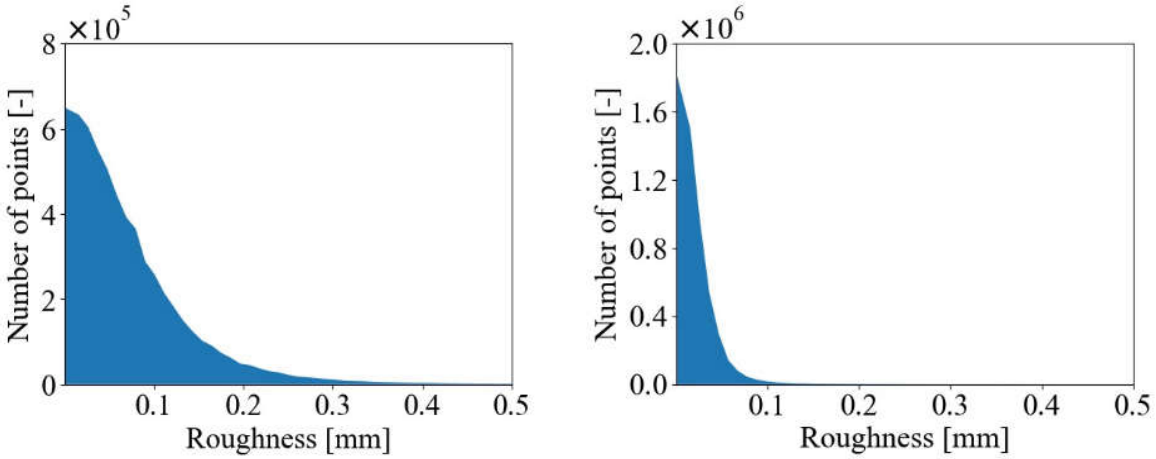

Figure 20. Combined diagrams of surface roughness for all the modules scanned form **a**) the top, and **b**) from the bottom.

The last value measured was the precision of the placement of the connectors. The determination of connector positions and the process of their installation during the module production were carried out manually, which affected their accuracy. The appearance of some displacements was also noticed during the printing of the second layer of the module. The accuracies of connector placing positions were measured as the distance

 doi:10.20944/preprints202203.0228.v1

between the planes of the corresponding connectors of the scanned and the designed modules. Since these measurements should give the same results for the scans from the top and the bottom of the modules, only the top scans were analyzed.

Error! Reference source not found. presents the results of measuring for one of the scanned modules. The arrows show the direction of connector displacements in the printed modules, and the numbers represent the values of the corresponding displacements in *mm*. As can be seen from the figure, the connectors were located with a rather large error. The fact that they are displaced in different directions indicates that the main reason for this is inaccuracies associated with manual installation, rather than displacement of the connectors during the printing of the second layer of the module. Since the module manufacturing technology proposed in Section 3 is focused on full automation, and in the future it is assumed that the placement of the connectors will be carried out by a robot, thus, this problem is not worth further attention.

Preprints (www.preprints.org) | NOT PEER-REVIEWED | Posted: 16 March 2022 doi:10.20944/preprints202203.0228.v1

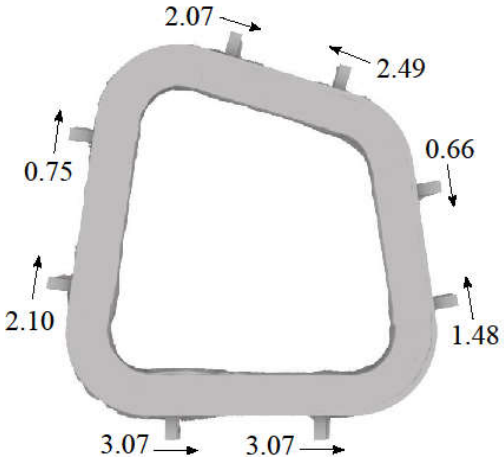

Figure 21. Example of measurement of accuracy of connector installation. Distances are shown in mm.

Error! Reference source not found. presents average results of geometric accuracy, surface roughness, and connector placement error for all the scanned modules. Average connector placement error was calculated as an average of the absolute values of all the measured values.

Table 3. Average results of printed module geometry analysis.

Scanned side	Average geometric inaccuracy [mm]	Average surface roughness [mm]	Average connector placement error [mm]
Top	2.22	0.0745	2.34
Bottom	1.95	0.0234	-

7.3. ConDIT 1.0 assembly

Upon completion of scanning of all modules produced, the demonstrator was assembled. To simplify the assembling process, at first, all the modules were connected in groups of four modules, as shown in **Error! Reference source not found.**a. Thus, half of all connections were completed, and the resulting groups were lightweight enough for subsequent assembly. The use of a bolted connection between the modules made it possible to connect all the modules to each other, despite the previously identified inaccuracies in the connectors' positioning. Half constructed ConDIT 1.0 and fully assembled demonstrator, hung on a crane, are presented in **Error! Reference source not found.**b and **Error! Reference source not found.**c, respectively.

Preprints (www.preprints.org) | NOT PEER-REVIEWED | Posted: 16 March 2022 doi:10.20944/preprints202203.0228.v1

a) b) c)

Figure 22. ConDIT 1.0 assembling process.

8. Conclusion

The authors have first suggested a new, highly automated method for creating grid-shell structures from variable modules. To prove the concept, a demonstrator – ConDIT 1.0 was designed and constructed. It consisted of 3D printed frame modules made of strain-hardening cement-based composite (SHCC). The main conclusions of the work can be summarized as follows:

- The results of the mechanical tests of the 3D printed SHCC samples confirmed the choice of this material as adequate for producing rims of modules within the suggested technology. This holds true also with respect to transferring the forces from the connectors to the modules' rims.
- Metal pins provided a good bond with SHCC and can be used in subsequent connector designs. Such designs should enable minimization of the distance between the adjoining modules.
- The results of structured-light scanning of the modules indicated the need for further work to improve the accuracy in their production. Surface roughness was another observed issue that need be solved to allow a closer connection between modules. In future work both problems should be resolved by upgrading the nozzle, modifying printing parameters, and improving the printed material formulation. It is also planned to eliminate errors in the placement of connectors by automating the process. As a transitional stage from manual to fully automated installation, it will also be possible to highlight the exact locations of the connectors using a laser mounted on a 3D printer.
- Despite the geometric imperfections observed, the successful completion of the ConDIT 1.0 proves the possibility of the adoption of 3D printing technology with novel fiber-reinforced types of concrete for the creation of shell structures from modules.

As the next step, the authors aim to pursue further the implementation of the proposed approach and plan to create a shell structure from modules with infill, reinforced with textile meshes.

Acknowledgments: This paper is part of the first author's PhD dissertation. The authors would like to thank the German Research Foundation (Deutsche Forschungsgemeinschaft – DFG) for financial support of the project "Adaptive Concrete Diamond Construction (ACDC)", project number 424057211, within the Priority Program "Adaptive modularized constructions made in flux" (SPP 2187).

Gefördert durch die Deutsche Forschungsgemeinschaft (DFG) – Projektnummer 424057211 – im Rahmen vom Schwerpunktprogram "Adaptive Modulbauweisen mit Fließfertigungsmethoden“ (SPP 2187).

References

[1] J. Hegger, M. Curbach, A. Stark, S. Wilhelm, and K. Farwig, “Innovative design concepts: Application of textile reinforced concrete to shell structures,” *Struct. Concr.*, vol. 19, no. 3, pp. 637–646, 2018, doi: 10.1002/suco.201700157.

[2] G. Tang and R. Pedreschi, “Gridshell as Formwork: Proof of Concept for a New Technique for Constructing Thin Concrete Shells Supported by Gridshell as Formwork,” *J. Archit. Eng.*, vol. 26, no. 4, p. 04020036, 2020, doi: 10.1061/(asce)ae.1943-5568.0000430.

[3] B. Kromoser and J. Kollegger, “Efficient construction of concrete shells by Pneumatic Forming of Hardened Concrete: Construction of a concrete shell bridge in Austria by inflation,” *Struct. Concr.*, vol. 21, no. 1, pp. 4–14, 2020, doi: 10.1002/suco.201900169.

[4] D. Veenendaal and P. Block, “Design process for prototype concrete shells using a hybrid cable-net and fabric formwork,” *Eng. Struct.*, vol. 75, no. 2014, pp. 39–50, 2014, doi: 10.1016/j.engstruct.2014.05.036.

[5] M. Antonucci and S. Nannini, “Through history and technique: Pier luigi nervi on architectural resilience,” *Archit. Hist.*, vol. 7, no. 1, pp. 1–13, 2019, doi: 10.5334/ah.297.

[6] V. Maneval, “Truss Wall House – Ushida Findlay Architects JAPON,” 2017. http://www.bubblemania.fr/en/truss-wall-house-1993-machida-city-tokyo-japon/.

[7] W. J. Hawkins *et al.*, “Flexible formwork technologies – a state of the art review,” *Struct. Concr.*, vol. 17, no. 6, pp. 911–935, 2016, doi: 10.1002/suco.201600117.

[8] H. Isler, “Concrete Shells Derived from Experimental Shapes,” *Struct. Eng. Int.*, vol. 4, no. 3, pp. 142–147, 1994, doi: 10.2749/101686694780601935.

[9] J. Chilton, “Form-finding and fabric forming in the work of Heinz Isler,” *Proc. Second Int. Conf. Flex. Formwork, ICFF*, pp. 27–29, 2012.

[10] J. Brennan, R. Pedreschi, P. Walker, and M. Ansell, “The potential of advanced textiles for fabric formwork,” *Proc. Inst. Civ. Eng. Constr. Mater.*, vol. 166, no. 4, pp. 229–237, 2013, doi: 10.1680/coma.12.00052.

[11] M. Popescu, L. Reiter, A. Liew, T. Van Mele, R. J. Flatt, and P. Block, “Building in Concrete with an Ultra-lightweight Knitted Stay-in-place Formwork: Prototype of a Concrete Shell Bridge,” *Structures*, vol. 14, no. February, pp. 322–332, 2018, doi: 10.1016/j.istruc.2018.03.001.

[12] “Chapel Lomas de Cuernavaca, Mexico - architect Félix Candela.” https://customrodder.forumactif.org/t4351-chapel-lomas-de-cuernavaca-mexico-architect-felix-candela (accessed Jan. 29, 2021).

[13] M. Popescu *et al.*, “Structural design, digital fabrication and construction of the cable-net and knitted formwork of the KnitCandela concrete shell,” *Structures*, vol. 31, no. February 2020, pp. 1287–1299, 2021, doi: 10.1016/j.istruc.2020.02.013.

[14] T. Van Mele, T. Méndez Echenagucia, D. Pigram, A. Liew, and P. Block, “Ultralight, flexible formwork system for thin, textile-reinforced concrete shells,” pp. 50–53, 2018.

[15] B. Kromoser and P. Huber, “Pneumatic Formwork Systems in Structural Engineering,” *Adv. Mater. Sci. Eng.*, vol. 2016, 2016, doi: 10.1155/2016/4724036.

[16] M. Schneider, “Pneu and Shell: Constructing Free-Form Concrete Shells with a Pneumatic Formwork,” *Humaniz. Digit. Real.*, vol. 2, pp. 639–655, 2018, doi: 10.1007/978-981-10-6611-5_53.

[17] A. Pugnale and A. Bologna, “Dante Bini’s Form-Resistant Binishells,” *Nexus Netw. J.*, vol. 19, no. 3, pp. 681–699, 2017, doi: 10.1007/s00004-016-0323-7.

[18] D. Williamson, J. Orr, and D. Fulford, “Biogas dome construction using pneumatics,” *J. Constr. Dev. Ctries.*, vol. 22, no. 2, pp. 35–53, 2017, doi: 10.21315/jcdc2017.22.2.3.

[19] A. Pronk, T. Bullens, and T. Folmer, "A faesable way to make freeform shell structures," *Proc. Int. Assoc. Shell Spat. Struct. Symp. 2007*, 2007.

[20] P. C. Van Hennik and R. Houtman, "Pneumatic Formwork for Irregular Curved Thin Shells," *Text. Compos. Inflatable Struct. II*, pp. 99–116, 2008.

[21] van F. Herwijnen, van den A. . Bos, and van R. Hove, "Gewelven met BetonBallon. Duurzame bouwmethode dankzij materiaalbesparing," *Cement*, vol. 61, no. 4, pp. 16–19, 2009.

[22] G. Quinn and C. Gengnagel, "A review of elastic grid shells, their erection methods and the potential use of pneumatic formwork," *WIT Trans. Built Environ.*, vol. 136, no. October 2016, pp. 129–144, 2014, doi: 10.2495/MAR140111.

[23] B. Kromoser and J. Kollegger, "Pneumatic forming of hardened concrete - Building shells in the 21st century," *Struct. Concr.*, vol. 16, no. 2, pp. 161–171, 2015, doi: 10.1002/suco.201400057.

[24] B. Kromoser and J. Kollegger, "Building concrete shells without formwork and falsework," no. 1996, pp. 1–8, 2018.

[25] B. Kromoser, T. Pachner, C. Tang, J. Kollegger, and H. Pottmann, "Form Finding of Shell Bridges Using the Pneumatic Forming of Hardened Concrete Construction Principle," *Adv. Civ. Eng.*, vol. 2018, 2018, doi: 10.1155/2018/6309460.

[26] A. Pronk, R. Houtman, and M. Afink, "The reconstruction of the Philips-pavilion volume 1," *Proc. Conf. Sources Archit. form, Kuwait*, vol. 1, 2007, [Online]. Available: http://www.arch.mcgill.ca/prof/sijpkes/Downloads/paper kuweit arno pronk.pdf%5Cnhttp://www.tue.nl/en/university/departments/built-environment/the-department-of-the-built-environment/staff/detail/ep/e/d/ep-uid/20022091/ep-tab/4/.

[27] C. A. Battaglia, M. F. Miller, and S. Zivkovic, *Sub-Additive 3D Printing of Optimized Double Curved Concrete Lattice Structures*. Springer International Publishing, 2019.

[28] T. Méndez Echenagucia, D. Pigram, A. Liew, T. Van Mele, and P. Block, "A Cable-Net and Fabric Formwork System for the Construction of Concrete Shells: Design, Fabrication and Construction of a Full Scale Prototype," *Structures*, vol. 18, pp. 72–82, 2019, doi: 10.1016/j.istruc.2018.10.004.

[29] E. Vicenzino, G. Cuiham, V. H. Perry, D. Zakariasen, and T. S. Chow, "First Use of UHPFRC in Thin Precast Concrete Roof Shell for Canadian LRT Station," *PCI J.*, vol. 50, no. 5, pp. 50–67, 2005, doi: 10.15554/pcij.09012005.50.67.

[30] J. G. Teng, "Steel-Concrete Composite Shells for Enclosing Large Spaces," no. 1998.

[31] S. Oesterle, A. Vansteenkiste, and A. Mirjan, "Zero Waste Free-Form Formwork," no. Figure 1, pp. 258–267, 2010.

[32] F. Huijben, "Vacuumatic formwork: a novel granular manufacturing technique for producing topology-optimised structures in concrete," *Granul. Matter*, vol. 18, no. 2, pp. 1–8, 2016, doi: 10.1007/s10035-015-0602-0.

[33] L. Enrique, P. Cepaitis, D. Ordoñez, and C. Piles, "CASTonCAST: Architectural freeform shapes from precast stackable components," *VLC Arquit. Res. J.*, vol. 3, no. 1, p. 85, 2016, doi: 10.4995/vlc.2016.4291.

[34] "Lluis Enrique, On Making Complex Things Simple," *L'Architecture d'Aujourd'hui*. https://www.larchitecturedaujourdhui.fr/making-complex-things-simple/?lang=en.

[35] C. Raun, M. K. Kristensen, and P. H. Kirkegaard, "Flexible Mould for Precast Concrete Elements," *Int. Assoc. Shell Spat. Struct. Symp.*, pp. 36–51, 2010.

[36] C. Raun and P. H. Kirkegaard, "Adaptive mould - A cost-effective mould system linking design and manufacturing of double-curved GFRC panels," *17th Int. Congr. GRCA*, no. September, p. 7, 2014, [Online]. Available: https://grca.org.uk/pdf/congress-2015/03 Adaptive mould - A cost-effective mould system linking design and manufacturing of double-curved GFRC panels.pdf.

[37] A. Pronk, A. Seffinga, H. el Ghazi, and N. Schuijers, "Flexible mould by the use of spring steel mesh," *Proc. Int. Assoc. Shell Spat. Struct.*, no. August, 2015.

[38] A. Pronk, I. Van Rooy, and P. Schinkel, "Double-curved surfaces using a membrane mould," *Proc. Int. Assoc. Shell Spat. Struct. Symp. 2009, Val.*, no. October, pp. 618–628, 2009.

[39] S. Hickert and U. Knaack, "Evaluation of free-form concrete architecture, moulding systems and their technical potentials,"

J. Facade Des. Eng., vol. 3, no. 3–4, pp. 273–288, 2016, doi: 10.3233/fde-160045.

[40] S. Grünewald, B. Janssen, H. R. Schipper, K. J. Vollers, and J. C. Walraven, "Deliberate deformation of concrete after casting," 2012.

[41] H. R. Schipper and B. Janssen, "Curving Concrete – A Method for Manufacturing Double Curved Precast Concrete Panels using a Flexible Mould Theoretical research," no. May 2015, 2015.

[42] S. Peters *et al.*, "Precast concrete shells: a structural challenge," 2017.

[43] B. Bell, N. Barnes, A. Ede, and T. C. Read, "Casting Non-Repetitive Geometries With Digitally Reconfigurable Surfaces," *ACADIA 2014 Des. Agency Proc. 34th Annu. Conf. Assoc. Comput. Aided Des. Archit.*, pp. 453–462, 2014.

[44] H. Schipper, S. Grunewald, P. Eigenraam, P. Raghunath, and M. Kok, "Production of curved precast concrete elements for shell structures and free-form architecture using the flexible mould method," pp. 1–12, 2014.

[45] M. Hoppermann, H. Reuvers, P. Nap, and B. Van Overveld, "Design to Installation of a free-form roof cladding with a flexible mould. The building of the public transport terminal Arnhem," *IASS 2015 Amsterdam Symp. Futur. Visions – ProRail Station. Netherl.*, no. August, pp. 1–13, 2015, [Online]. Available: https://www.ingentaconnect.com/content/iass/piass/2015/00002015/00000010/art00001.

[46] A. Pronk, T. Lusing, and R. H. P. G. Versteeg, "The VaCo Mould, a research about a new moulding principle for double curved concrete panels," *Int. Soc. Flex. Formwork*, no. 2015, 2015.

[47] "Adapa Company." https://adapa.dk/.

[48] H. R. Schipper *et al.*, "Kine-Mould: Manufacturing technology for curved architectural elements in concrete," no. August, 2015.

[49] S. Lim, R. A. Buswell, P. J. Valentine, D. Piker, S. A. Austin, and X. De Kestelier, "Modelling curved-layered printing paths for fabricating large-scale construction components," *Addit. Manuf.*, vol. 12, no. June, pp. 216–230, 2016, doi: 10.1016/j.addma.2016.06.004.

[50] J. H. Lim, Y. Weng, and Q. C. Pham, "3D printing of curved concrete surfaces using Adaptable Membrane Formwork," *Constr. Build. Mater.*, vol. 232, p. 117075, 2020, doi: 10.1016/j.conbuildmat.2019.117075.

[51] C. Borg Costanzi, Z. Y. Ahmed, H. R. Schipper, F. P. Bos, U. Knaack, and R. J. M. Wolfs, "3D Printing Concrete on temporary surfaces: The design and fabrication of a concrete shell structure," *Autom. Constr.*, vol. 94, no. May, pp. 395–404, 2018, doi: 10.1016/j.autcon.2018.06.013.

[52] V. C. Li *et al.*, "On the emergence of 3D printable Engineered, Strain Hardening Cementitious Composites (ECC/SHCC)," *Cem. Concr. Res.*, vol. 132, no. January, p. 106038, 2020, doi: 10.1016/j.cemconres.2020.106038.

[53] H. Ogura, V. N. Nerella, and V. Mechtcherine, "Developing and testing of Strain-Hardening Cement-Based Composites (SHCC) in the context of 3D-printing," *Materials (Basel).*, vol. 11, no. 8, pp. 1–18, 2018, doi: 10.3390/ma11081375.

[54] V. Mechtcherine, A. Michel, M. Liebscher, K. Schneider, and C. Großmann, "Mineral-impregnated carbon fiber composites as novel reinforcement for concrete construction: Material and automation perspectives," *Autom. Constr.*, vol. 110, no. September 2019, p. 103002, 2020, doi: 10.1016/j.autcon.2019.103002.

[55] V. Mechtcherine, "Towards a durability framework for structural elements and structures made of or strengthened with high-performance fibre-reinforced composites," *Constr. Build. Mater.*, vol. 31, pp. 94–104, 2012, doi: 10.1016/j.conbuildmat.2011.12.072.

[56] M. Lieboldt and V. Mechtcherine, "Capillary transport of water through textile-reinforced concrete applied in repairing and/or strengthening cracked RC structures," *Cem. Concr. Res.*, vol. 52, pp. 53–62, 2013, doi: 10.1016/j.cemconres.2013.05.012.

[57] K. Schneider, A. Michel, M. Liebscher, L. Terreri, S. Hempel, and V. Mechtcherine, "Mineral-impregnated carbon fibre reinforcement for high temperature resistance of thin-walled concrete structures," *Cem. Concr. Compos.*, vol. 97, pp. 68–77, 2019, doi: 10.1016/j.cemconcomp.2018.12.006.

[58] G. Tang, "An overview of historical and contemporary concrete shells, their construction and factors in their general

 doi:10.20944/preprints202203.0228.v1

disappearance," *Int. J. Sp. Struct.*, vol. 30, no. 1, pp. 1–12, 2015, doi: 10.1260/0266-3511.30.1.1.

[59] S. Dallinger and J. Kollegger, "Construction method for shell structures made of planar precast concrete components," *CPI - worldwide*, 2012. https://www.cpi-worldwide.com/us/journals/artikel/3606/construction-method-for-shell-structures-madeof-planar-precast-concrete-com.

[60] J. Kollegger, B. Kromoser, and S. Dallinger, "The building of ice and concrete shells by employing pneumatic formwork," *Second Int. Conf. Flex. Formwork*, no. June 2012, 2012.

[61] D. Lordick, "Eine Bugholzkonstruktion ganz ohne Kleber und Metall.," 2020. https://tu-dresden.de/tu-dresden/newsportal/news/eine-bugholzkonstruktion-ganz-ohne-kleber-und-metall.

[62] S. Ghourchian, M. Butler, M. Krüger, and V. Mechtcherine, "Modelling the development of capillary pressure in freshly 3D-printed concrete elements," *Cem. Concr. Res.*, vol. 145, 2021, doi: 10.1016/j.cemconres.2021. 106457.